PCCP

Accepted Manuscript

ROYAL SOCIETY OF CHEMISTRY

www.rsc.org/pccp

Physical Chemistry Chemical Physics
CREATED USING THE RSC LaTeX PCCP ARTICLE TEMPLATE – SEE www.rsc.org/electronicfiles FOR DETAILS
ARTICLE TYPE www. rsc.org/xxxxxx | XXXXXXXX

Aqueous solutions of tetraalkylammonium halides: ion hydration, dynamics and ion-ion interactions in light of steric effects

Debsindhu Bhowmik,[a,‡] Natalie Malikova,[a,x*] Guillaume Mériguet,[b] Olivier Bernard, [b] José Teixeira, [a] and Pierre Turq [b]

Received Xth XXXXXXXXXX 20XX, Accepted Xth XXXXXXXXX 20XX
First published on the web Xth XXXXXXXXXX 200X
DOI: 10.1039/b000000x

Molecular simulations have allowed us to probe the atomic details of aqueous solutions of tetramethylammonium (TMA) and tetrabutylammonium (TBA) bromide, across a wide range of concentrations (0.5 to 3-4 molal). We highlight the space-filling (TMA^+) versus penetrable (TBA^+) nature of these polyatomic cations and its consequence for ion hydration, ion dynamics and ion-ion interactions. A well-established hydration is seen for both TMA^+ and TBA^+ throughout the concentration range studied. A clear penetration of water molecules, as well as counterions, between the hydrocarbon arms of TBA^+, which remain in an extended configuration, is seen. Global rotation of individual TBA^+ points towards isolated rather than aggregated ions (from dilute up to 1m concentration). Only for highly concentrated solutions, in which inter-penetration of adjacent TBA^+s cannot be avoided, does the rotational time increase dramatically. From both structural and dynamic data we conclude that there is absence of hydrophobicity-driven cation-cation aggregation in both TMABr and TBABr solutions studied. The link between these real systems and the theoretical predictions for spherical hydrophobic solutes of varying size does not seem straight forward.

1 Introduction

In the field of ionic solutions, those containing tetraalkylammonium (TAA, $N(C_nH_{2n+1})_4^+$) cations occupy a very specific position. These cations, considered as the archetypal hydrophobic cations, bring into play both charge and hydrophobicity, a combination of great importance in many environmental and biological processes. As such they are also widely used in phase transfer catalysis, involving an aqueous and an organic phase. The series of small symmetric TAA cations, most often with halide counterions, has been at the core of numerous studies to investigate the effect of hydrophobicity on ion hydration and ion-ion interactions in aqueous solutions, for reviews see [1–3]. The hydrophobic character for TAAs is considered tuneable via the length of the four alkyl chains attached to the central nitrogen atom. The first four members of the TAA series (referred to from now on as TMA^+, TEA^+, TPA^+ and TBA^+, from the smallest to the largest cation) have been studied most extensively. They show high solubility limits, comparable to alkali halides, considered as their purely electrostatic analogues [4].

Despite the wealth of past studies, as of today we are unable to link the thermodynamic and structural data for TAA ions in solution into a coherent picture. Thermodynamic data shows clearly that the transfer of TAA cations from aqueous to non-aqueous solutions is accompanied by an increasingly negative Gibbs free energy as the cation size increases (TMA^+ features however a positive value), which put forward the idea of larger TAAs being "hydrophobic ions". Moreover, this Gibbs free energy is dominated by an increasingly positive entropy term [3]. To explain these findings, several structural studies have focused on providing evidence for a) increased structuring of water in the vicinity of TAA ions, perhaps leading all the way to clathrate formation, and b) formation of cation-cation pairs, as the cation size increases. Unfortunately the evidence for either one of them is not clearly established. Neutron diffraction [5–7], microscopic simulation [8,9] as well as dynamic studies by NMR and neutron scattering [10–15], conclude against increased water structuring and see no clathrate formation, with the possible exception of TBA^+ in the low temperature regime only [12]. At the same time, neutron diffraction and microscopic simulation agree on the unusual tangential orientation of water molecules around individual TAA ions, in stark contrast to alkali cations [8,9,16]. Defining θ as the angle between the vector joining the cation (central N atom in case of TAA) to the oxygen atom of a water molecule and the dipole moment vector of the same water molecule, tangential orientation refers to cases when these two vectors are at or close to 90 degrees. This is the case for TAA ions and contrast with θ

[a] *Laboratoire Léon Brillouin, UMR CEA-CNRS 12, CEA Saclay, 91191 Gif-sur-Yvette, France.*
[b] *Sorbonne Universités, UPMC Univ Paris 06, CNRS, UMR 8234, PHENIX, F-75005, Paris, France.*
‡ *Present address: Department of Physics and Astronomy, Wayne State University, 666 W Hancock Street, Detroit, MI 48201.*
x *Present address: Sorbonne Universités, UPMC Univ Paris 06, CNRS, UMR 8234, PHENIX, F-75005, Paris, France, natalie.malikova@upmc.fr*

close to zero in case of alkali ions. Within the microscopic picture, this tangential orientation of water molecules has since been referred to as "hydrophobic hydration". However, a direct correspondence of this feature and the thermodynamic classification is not easy, as even the TMA^+ (thermodynamically hydrophilic) features this type of unusual hydration. Regarding cation-cation aggregation, small angle neutron scattering (SANS) and neutron diffraction do not support it in TAA halide solutions, though they give evidence for instances where adjacent TAA cations are not separated by water[17–19]. Any inferred TAA-TAA association is clearly very weak in comparison to that seen for larger phenyl containing phosphonium based cations in aqueous solution, where phenyl-phenyl specific interaction is likely to play a non-negligible role[20]. On the contrary, some recent results by small angle X-ray scattering and simulation[21] as well as femtosecond infrared spectroscopy[22] are interpreted as giving evidence for TAA-TAA aggregation or cluster formation.

It is clear that TAA halide solutions have some distinct features when compared to solutions of alkali halides. However, which of these features can truly be assigned to their hydrophobicity? Whereas theoretical studies concerned with hydrophobic solutes have the power to tune a single parameter, such as the solute size[23], clearly, when it comes to real systems, the transition from an alkali cation towards a TAA cation is far from an addition of a single parameter. This is obvious from the polyatomic nature of TAA cations, their size and the finite distribution of charge among the atoms. Without resorting to hydrophobicity, these steric and geometrical aspects play a significant role by themselves. As has been highlighted recently for example, it is the substantial excluded volume fraction occupied by TAA-resembling ions in moderate to concentrated solutions that is the reason behind the slowing down of water dynamics observed, rather than any intrinsic hydrophobicity effect of the ions present[24]. This reasoning revives the obstruction effect mentioned already in the past[11].

Motivated by highlighting the steric/geometrical aspects of TAA ions in aqueous solutions, we have resorted to microscopic simulations with a fully-atomic model of the ions (explicit H atoms). We study a range of concentrations, 0.5 to 3-4 on the molality scale, which includes the moderate to concentrated systems studied experimentally in the past. The exact concentrations chosen for a given system were guided by the concentration of a single hydration shell per TAA cation, which has been used extensively as a reference[7,8,11,25]. Importantly, we report upon both structural *and* dynamic properties of the ions, we highlight their space-filling (TMA^+) versus penetrable (TBA^+) nature and its consequence for ion hydration, ion dynamics and ion-ion interactions.

2 Simulation Techniques

Classical molecular dynamics (MD) simulations (using the code DL POLY 2.18[26]) were performed on a series of aqueous solutions of TMABr, TBABr and NaBr, spanning a range of concentrations. The overview of simulated systems is given in Table 1. An all atom (explicit N, C and H atoms), flexible (bond stretch, bond bending, dihedral interaction), non-polarizable model was taken for the TMA^+ and TBA^+ ions. The non-bonding interactions in the system were described via the Coulombic and Lennard-Jones (LJ) potentials, with the use of Lorentz-Berthelot mixing rules for the LJ parameters[27]. Individual atomic charges within the TMA^+ and TBA^+ ions were determined by the restrained electrostatic potential (RESP) fitting of Hartree-Fock results included in the Antechamber library of the AMBER code[28–32]. Other interaction parameters for these ions were taken directly from the Generalized Amber Force Field (GAFF)[28–32]. Bromide and sodium ion parameters were taken from literature[33–37] and rigid SPC/E model was used for water[38]. A compilation of parameters used in our simulations is provided in Supplementary Information.

For any given system, a cubic simulation box was filled initially with regularly spaced ions and water molecules (at random orientations). Three dimensional periodic boundary conditions were used, a cutoff radius for short-range interactions was half of the box-size, long-range part of the electrostatic interaction was evaluated using the 3D Ewald sum[39], SHAKE algorithm[27,40] was used for rigid SPC/E water molecules. The initial configuration was equilibrated in NpT ($p = 1$ atm, $T = 298$ K) and then NVT ensembles. As an initial check of the interaction potentials, the simulated density obtained from the NpT equilibration was compared to the available experimental data. The comparison is given in Supplementary Information, the difference in simulated and experimental values is $<0.2\%$. A production run was further carried out in the NVE ensemble, with a total length of at least 3.4 ns and a timestep of 1 fs. Individual atomic trajectories were saved every 0.1 ps, producing at least 34×10^3 frames in total. Trajectories were then analysed using nMoldyn[41,42] to obtain both static and dynamic properties of ions and water molecules.

3 Results

3.1 Ion hydration

We consider at first the hydration of ions in TMABr, TBABr and NaBr aqueous solutions and its concentration dependence. Figure 1 shows the radial distribution functions between central nitrogen atoms of the cation and oxygen atoms of water molecules, g_{NO_w}, for TMABr and TBABr solutions. We observe that g_{NO_w} for TMABr solutions is very much concen-

tration independent in the range shown. The first prominent peak is centered on 4.4 Å, with the corresponding coordination number of 25 water molecules. Thus we see a well-defined first hydration shell for TMA^+, which has been suggested previously by MD simulation for a very dilute solution using a 5-site TMA model (no explicit H atoms)[9], and also reported by neutron diffraction at higher concentration[16]. We see that this hydration sphere survives with almost no modification across a wide concentration range, up to and including the one hydration sphere limit. A weaker secondary shell is also seen here, centered at a distance of 7.5 Å. The g_{NO_w} functions for TBABr show, between 4 and 9 Å, a rather complicated structure, but the notable features are at comparable distances to those for TMABr. The first part, up to 6.2 Å, corresponds now to water molecules which are closer than the outermost H atoms of TBA^+ (their position is indicated by the vertical dashed line). In the $g(r)$ representation, the intensity of this peak is highly concentration dependent, but should not be interpreted automatically as a significant change in the number of these "inner" water molecules: their number varies slightly from 20 H_2O at 0.06 m down to 17 at 1.98 m (and then fast to 13 at 3.96 m). The strong intensity variation of the first $g(r)$ peak is a consequence of the significant volume fraction occupied by the TBA^+ ions in these solutions (from 2% at 0.06m to 50% at 3.96m), which leads to strong variation in the number density of water molecules, i.e. the $g(r)$ normalisation factor.The well-defined peak between 6.2 and 10 Å in the $g(r)$ shows on the contrary more constant an intensity, thus the relative density of water molecules in this region is permanently in excess of the average density (the corresponding coordination number is 100 water molecules at 0.06m and 50 at 3.96m).

Comparing the details of water orientation between TMABr, TBABr and NaBr (at 1m concentration), we confirm the close to tangential orientation in case of TMA^+ and TBA^+ (see Supplementary Information for the relevant graphs). In addition, we observe that this orientation is lost in the second hydration shell of TMA^+. It is retained in case of the second hydration shell of TBA^+, though this is most probably the effect of an adjacent TBA^+. Hydration of Br^- in the TMABr and TBABr solutions is similar to that of NaBr (data not shown). The coordination number found for alkali halide solutions (=7.5) is also found for TMABr and TBABr solutions, it remains almost constant up to concentrations corresponding to the respective one hydration sphere limits, beyond which the anion is loosing its usual coordination.

3.2 Ion-Ion interactions

Ion-ion correlation functions were inevitably poorer in statistics than ion-water correlation functions, due to the finite number of ions in the simulation box. In the following we thus had to omit data for some of the lower concentrations. Figure 2 shows the radial distribution functions between the nitrogen atom of the cation and Br^- (g_{NBr}) for the series of TMABr and TBABr solutions as a function of concentration. The main feature in the g_{NBr} for TMABr is a well-defined intense peak centered at 5 Å, the position of which is concentration independent and is 2.8 Å away from the hydrogen atoms of the TMA^+ (position of these H atoms is indicated by a vertical dashed line in the figure). Interestingly, the g_{NBr} for TBABr solutions features its first peak at the same distance as for TMABr solutions, i.e. at 5Å. Br^- corresponding to this first peak are closer to the nitrogen atom than the outermost H atoms, though further than the next inner layer of H atoms. The penetration of Br^- inbetween the last quarter of the hydrocarbon arms of the TBA^+ is thus made clear, a similar observation was reported in the previous section for water molecules themselves. The coordination number of these inner Br^- ions is about 1/3 and note that this increases dramatically as we move above the one hydration sphere concentration, we shall discuss this point later. Further out, the g_{NBr} features a broader double peak.

Figure 3 features the radial distribution functions between the nitrogen atoms of cations for TMABr and TBABr solutions, with dotted and dashed-dotted vertical lines indicating, respectively, position of the outermost hydrogen atoms of the cation and the first layer of water oxygen atoms (first peak position in g_{NOw}). A distinct TMA-TMA correlation peak centered at 8.4 Å is visible at the one hydration sphere concentration. It persists as the system is diluted, with no change in position, though decreasing in intensity. This peak lies further than the first correlation peak both in g_{NOw} and g_{NBr}. Considering the position of the hydrogen atoms on a single TMA^+, the first TMA-TMA correlation peak does not correspond to two adjacent TMA^+s in contact, rather two TMA^+s sharing a hydration shell, but possibly also a Br^- counterion. In contrast to TMA^+, a broad TBA-TBA correlation peak is visible only at the highest concentration considered (3.96m, significantly above the one hydration sphere limit). At the one hydration sphere limit (1m), the $g(r)$ shows very little correlation. Considering again the position of the outermost hydrogen atoms on a single TBA^+ (6.2 Å), the peak observed at 3.96m has to correspond to interpenetration of the arms of the adjacent TBA^+s. Note that the hydrocarbon arms are rather rigid and do not show any bending as the concentration is increased. This is made obvious from our MD simulations from the radial distribution functions of the terminal carbon atoms around the central N atom (data not shown). Moreover, we have also observed this experimentally via small angle neutron scattering[43]. In case of such extended arms, the interpenetration of adjacent TBA^+s seems sterically very much feasible as they are far from space filling objects, as was made obvious already from the corresponding g_{NOw} and g_{NBr}. In the space between adjacent TBA^+s there is again non-zero density of water molecules and possibly also Br^- counterions, as in the

case of two adjacent TMA^+s. This applies for all concentrations studied.

3.3 Diffusion

The translational diffusion coefficients of TAA ions and water in our solutions have been calculated from the mean square displacements (MSD) of the central N atoms for the ions and O atoms for water, according to:

$$MSD(t) = \left\langle |\mathbf{r}_i(t) - \mathbf{r}_i(0)|^2 \right\rangle = 6Dt \quad (1)$$

Figure 4 shows our simulated translational diffusion coefficients of cations and water molecules in a series of TMABr and TBABr solutions, together with a compilation of other experimental and simulated data available from the literature. Note that in MD, the size of the system has an a priori measurable effect on the measured diffusion coefficients[44,45]. We have however tested this for the 1 m concentration of TBABr with three box sizes and no dependence has been observed, certainly because of the high viscosity of the system. For comparison between data from different techniques, note that deuterated water is often necessary to measure experimentally the diffusion coefficient of the hydrogen containing cations (in NMR and neutron scattering in particular), while tracer experiments (and simulations) are carried out in light water. Solvent deuteration leads to a difference in the solvent viscosity (D_2O/H_2O viscosity ratio is 1.23 at 298 K), which marks its effect only at low TAABr concentrations: tracer data consistently above NMR data at low concentration in Figure 4 a) and b). Already at 1m concentration, this effect seems however insignificant.

3.4 Local and internal motion of TAA cations

We have chosen to concentrate on two types of local/internal motions of the TAA ions: 1) global cation rotation, also referred to in literature as the tumbling motion and 2) rotation of the terminal methyl groups, since they are both well documented in the literature, mostly using experimental techniques. Global cation rotation was probed using the mean square displacement (MSD) of the α C atoms (directly bonded to the central N atom) relative to the central N atom. We considered this to be the most accurate estimate, as the effects of arm bending on this MSD play a minimal role. Methyl group rotation was treated in a similar manner, from the mean square displacement of H atoms relative to adjacent C atoms, *while* correcting for any possible global cation rotation. This correction is especially important when the characteristic time of global rotation is similar to that of the methyl group rotation. We shall see that this is the case for TMA^+, contrary to TBA^+.

For rigid molecules, rotational dynamics is evaluated from the orientational correlation function $C_\ell(t) = \langle P_\ell(\mathbf{u}(0)\cdot\mathbf{u}(t))\rangle$, where $\mathbf{u}$ is a unit vector indicating the orientation of the molecule and P_ℓ the ℓ-rank Legendre polynomial[46,47]. For a pure global rotational diffusion, we obtain $C_\ell(t) = e^{(-\ell(\ell+1)D_{\rm rot}t)}$, where $D_{\rm rot}$ is the rotational diffusion coefficient. The relative MSD displacement is related to $C_1(t)$ as follows

$$\begin{aligned} MSD(t) &= 2b_{\rm N-C}^2\left(1 - C_1(t)\right) \\ &= 2b_{\rm N-C}^2\left(1 - \mathrm{e}^{-2D_{\rm rot}t}\right) \\ &= 2b_{\rm N-C}^2\left(1 - \mathrm{e}^{-2t/\tau_{\rm rot}}\right) \end{aligned} \quad (2)$$

where $b_{\rm N-C}$ is the length of the N–C bond. Since it has been derived for rigid molecules, the above equation does not apply to short correlation times ($t < 1$ ps), where the fast vibration and distortion of the bonds play a significant role. Figure 5 summarizes the relative MSD obtained for the case of global cation rotation for both TMA^+ and TBA^+ and it is well modelled by Equation 2. For TBA^+, global rotation is seen to be strongly concentration dependent, but only beyond the one-hydration sphere limit (0.99m). The characteristic time is $\tau_{\rm rot} = 0.54$ ns for infinite dilution up to 1 m and then reaches $\tau_{\rm rot} = 3.1$ ns at 3.96 m. The orientational dynamics of every carbon and hydrogen atom inside TBA^+ was investigated for selected TBABr systems (data not shown). For any atom in the two most inner methylene (CH_2) groups, the characteristic times were close to the global rotation time, as determined above. This indicates the significant stiffness of the TBA^+ core. The global rotation for TMA^+ in the range studied (up to and including its one-hydration sphere limit) is found to be concentration independent, but with a much smaller characteristic time, $\tau_{\rm rot} = 5 \pm 1.5$ ps.

As for methyl dynamics, two main classical descriptions exist: a continuous diffusion on a circle and a threefold jump process[47–49]. The corresponding relative MSD, once corrected for the global rotation, can be expressed in a similar manner to equation 2 :

$$MSD(t) = 2b_{\rm C-H}^2 \sin^2\phi\left(1 - \mathrm{e}^{-D_{\rm rot}t}\right) = 2b_{\rm C-H}^2 \sin^2\phi\left(1 - \mathrm{e}^{-t/\tau_{\rm rot}}\right) \quad (3)$$

where $b_{\rm C-H}$ is the length of the C–H bond and $\phi = 109°5$ the angle between the C–H bonds. For a jump process, the characteristic time between jumps is $\tau_{\rm j} = \frac{3}{2}\tau_{\rm rot}$[48,50]. MSD behaviour cannot distinguish between the two types of methyl dynamics, but it is still possible to compare TMA^+ and TBA^+. Relative MSD for terminal methyl group rotation shows minimal concentration dependence for both TBA^+ and TMA^+ (see Supplementary information), with somewhat different mean characteristic times $\tau_{\rm rot}$ of 6 ps and 2 ps respectively.

4 Discussion

We shall now summarize our results on ion-hydration, ion-ion interactions and ion dynamics in TAABr solutions, putting them into context with previous literature.

Our MD results show TMA^+ hydration as a distinct layering of hydration shells (first shell containing approx. 25 water molecules), as in the case of simple monoatomic cations. We confirm the tangential orientation observed experimentally and in previous simulations[8,9,12,16]. We see that this orientation is lost in the second hydration shell of TMA^+. The well-defined first hydration shell of TMA^+ exists over a wide concentrations range, up to and including the single hydration layer reference, with very little variation in the coordination number. Hydration of TBA^+ is dominated by the fact that it is not an impenetrable species and that its hydrocarbon arms remain in an extended configuration across a wide concentration range. A rather constant number of water molecules (approx. 20) fills the space between the arms, the density of these "inner" water molecules is naturally the result of the space available and the interactions with the arms of TBA^+. Interestingly these molecules possess also close to a tangential orientation with respect to the central N atom.

The charge on any given TAA cation is crucial for hydration to occur and for the stability of the solution (removal of charges on TAA results, as expected, in demixing[21]). Where available in the literature, we see that charge distribution in the microscopic models of TAA cations has been a) +1 charge distributed equally over the four α C atoms irrespective of the length of the hydrocarbon arms[8,9] or b) charge more spread out along the hydrocarbon arms as in our model[28,51]. The difference between these charge distributions does not affect the water orientation observed, tangential is seen in all. For coarser models, the entire TAA cation considered as a single pseudoatom, this type of information is blurred and no preferential orientation is concluded[52]. Spatially extended and non-spherically distributed charge density on the cation seems then an important condition for the tangential configuration of water molecules. Apart from water molecules, the space between the arms of TBA^+ is also occupied by Br^- counterions (with a coordination number of 1/3 up to the 1.98m concentration). These counterions posses their full hydration shell of 7.5 water molecules up to the 1m concentration. Beyond this point it begins to be lost, certainly due to steric effects. Penetration of Br^- was previously seen in the case of TPA by simulation[28] and is consistent with the notion of penetration cation-anion pairs referred to earlier on the basis of dielectric spectroscopy measurements[53].

The extent of cation-cation aggregation in TAA halide solutions remains a widely-discussed topic, let us view the ion-ion correlation functions we have obtained by MD in light of this aspect. We may start by considering that cation-cation effective pair potentials in our solutions possess a) a short-range repulsive part due to steric effects, b) cation-cation electrostatic repulsion and c) a short-range attractive (hydrophobicity-driven) part. Regarding electrostatic repulsion, we note that in the highly concentrated solutions studied, it is screened over a few Å (the Debye screening length for 1 molar aqueous solution at 298K is only 3 Å). If cation-cation electrostatic repulsion was dominating we would expect to see the position of the first peak in g_{NN} to be concentration dependent. Further, assuming a simple model of the cations on a grid, the equilibrium cation-cation distance would be varying between 9.5Å and 14Å for 2.52m and 0.63m TMABr solutions (9.7Å and 30.1Å for 3.96m and 0.50m TBABr solutions). However, we observe no shift in the first peak of g_{NN} for both TMABr and TBABr solutions. Apart from the 3.96m TBABr system, the peak position is at smaller distances than what is predicted by the simple grid model. Thus the observed correlation peak reflects a short-range interaction, which, without any other knowledge, could have its origin either in short-range steric repulsion or short-range hydrophobic attraction.

At this point, the information on cation hydration seems of utmost importance and, as mentioned above, we report a well-established hydration of both TMA^+ and TBA^+ persisting throughout the whole concentration range considered. A hydrophobicity-driven cation aggregation would be accompanied by at least a partial loss of hydration water, but this is not observed. In case of TMA^+, considering the sizes of the "naked" and hydrated cation, we were brought to conclude that the clear TMA-TMA correlation peak at 8.4 Å does not correspond to two TMA^+s in contact but rather being separated by a hydration sphere, albeit incomplete, and possibly also a Br^- counterion. Thus we trace the first peak in g_{NN} to the short-range steric repulsion between partially hydrated TMA^+s. Further, comparing g_{NN} of TMABr and TBABr solutions at a given concentration (consider 1m), we observe a clear decrease in the first peak intensity as we move from TMA^+ to TBA^+. Indeed, even at 1m, there is only a very weak peak in the g_{NN} for TBABr. If hydrophobicity was the underlying interaction, we would expect the opposite trend, an increase in the correlation peak as we move to TBA^+. The observed intensity trend reflects in our opinion the relative hardness/softness of the short-range cation-cation steric repulsion and is consistent with the space-filling (hard) nature of the TMA^+ and penetrable (soft) nature of TBA^+. The transition from 0.99m to 3.96m for TBABr is then an interesting case. We observe finally a clear appearance of a TBA-TBA correlation, also a dramatic increase in TBA-Br correlation at 5 Å. Referring to the above simple model of TBA^+ ions on a regular grid, the transition 0.99m to 3.96m corresponds to a TBA-TBA separation decreasing from 13.0 to 9.7 Å. At 3.96m the TBA^+ are effectively at this predicted distance, they are closely packed, with partially inter-penetrated arms and coun-

terions as well as water molecules locked inside the region between the arms. This interpenetration is accompanied by a decrease in "inner" water molecules (from 17 to 13). The effective TBA-TBA potential is suddenly "harder", i.e. even more repulsive due to steric reasons, and a correlation peak appears in g_{NN}.

Overall, regarding cation-cation correlations, we observe some agreement but also differences from the available literature. Our results agree well with the distance of the most prominent peaks for both TMA-TMA and TBA-TBA correlations[21]. However, in terms of trends in peak intensities, the results clearly disagree. The only concentration for which we see a clear TBA-TBA correlation peak is only at 3.96m, while a clear TMA-TMA peak is present throughout the whole concentration range studied. Simulations in ref[21] refer to 1m concentration and show a strong TBA-TBA correlation, stronger than the TMA-TMA peak. This is an important point, as it is interpreted by the authors as evidence for hydrophobicity-driven TBA aggregation, with which our results seem inconsistent. More in line with our results are the data of Krienke et al, where the first two members of the TAA series were studied (TMA^+ and TEA^+)[51]. A clear decrease in the intensity of cation-cation correlation peaks was seen on transition from TMA^+ to TEA^+ (at roughly 0.6m concentration). Moreover, hypernetted chain (HNC) calculations made in conjunction with SANS experiments on TBABr aqueous solutions[18] result in a potential that leads to a very featureless TBA-TBA pair correlation function at 0.99m (data included in Figure 2 right). SANS is particularly sensitive to the signal from cation-cation correlations in TAABr solutions due to the high concentration of H atoms in TAA cations (yielding a good contrast with respect to the deuterated solvent) as well as their greater size in comparison to the anions. In order to assess whether the atomic configurations in our simulations reproduce scattering data from TBABr solutions, we were brought to compare directly the reciprocal space data from neutron scattering from ref[43] and those calculated from our simulations. This is another very pertinent test of the realistic nature of the force field used in our simulations. The comparison was made at 1m concentration and is featured in Figure 6. We see that our simulations reproduce very reliably the experimental neutron scattering data across a wide spatial range. Therefore, the same atomic configurations leading to a very featureless TBA-TBA $g(r)$ (Figure 2 right) can reproduce experimentally measured neutron scattering data. As detailed in ref[43], the neutron scattering data is dominated by the form factor of the individual TBA^+ ions at low Q values and by the broad solvent peak centered on Q=1.8 Å. The data shows no evidence of a strong TBA-TBA correlation peak and is in accord with previous literature using this technique[17–19]. Regarding other scattering techniques, reference[21] presents SAXS measurements for TAA halide solutions[21] showing an interesting evolution as a function of increasing TAA cation size: the gradual appearance of a correlation peak, centered at 0.8 $Å^{-1}$ for TBABr solution. In conjuction with the above-mentioned simulations from this reference, this peak is again taken as evidence for TBA-TBA aggregation. Interestingly, we were able to calculate the SAXS signal from our simulated TBABr system at 1m and are able to reproduce the observed peak (see Supplementary Information). The same atomic configurations that give rise to the SAXS peak show a very featureless TBA-TBA $g(r)$. In our opinion, the observed SAXS peak cannot reflect TBA-TBA aggregation. On the grounds of electronic density, it seems probable that this peak reflects primarily the correlations involving Br^- (anion-anion or anion-cation correlation or both), but not the cation-cation correlation.

Overall, on the basis of our simulated structural data, we see no evidence for cation-cation aggregation in the TMABr and TBABr solutions studied. This is further supported by the dynamic information we were able to obtain, more precisely the individual global ion rotation. For global ion rotation the compact versus penetrable nature of the two TAA cations could again have a clear effect. Up to the respective one hydration sphere limits, we observe a concentration independent global rotation for both TMA^+ and TBA^+. Beyond the 1m concentration, TBA^+ rotation is severely hindered and the origin is in the increasing inter-penetration of adjacent ions. This would not occur for the compact TMA^+ cation and we expect, beyond its one hydration sphere limit, a much weaker (if any) concentration dependence of its global rotation. Similarly, the behaviour of the terminal methyl groups is also affected by the difference in penetrability. For very similar interaction potentials, the characteristic times for methyl group rotation are indeed different (6ps and 2ps for TBA^+ and TMA^+ respectively). The environment for terminal methyl groups in TBA^+ is likely to be affected by the presence of water molecules (and counterions) penetrating between the hydrocarbon arms.

The observed evolution of TBA^+ global rotation from our simulations is supported by the available experimental data. The main source of experimental data regarding global rotation of TAA cations are NMR relaxation measurements, where we measure a correlation time τ_c, which for rotational diffusion is related to τ_{rot} according to $\tau_{rot} = 6\tau_c$[49]. Even if the decoupling of the different dynamics is not straightforward in this technique, the global rotation can often be extracted using reasonable approximations, since it is the slowest dynamic mode[49,54]. For low concentrations (< 0.05 mol L^{-1}) the measured correlation time for TBA^+ is in the range of 87-115 ps, depending on the exact concentration, counterion and nucleus probed[55–58]. A single measurement is available at high concentrations for TBACl solution (7.9m) giving a value of $\tau_c = 0.63$ ns. Taking into account the conversion factor of 6 between τ_c and τ_{rot}, these experimental values are indeed in a very good agreement with our simulations

and show the changes occurring beyond the single hydration sphere limit. Regarding TMA^+ rotation, experimental data suggest τ_c of the order of 5 ps at low concentrations, with only a small increase up to 5m concentrations (less than a factor of 1.5)[10,13,55,59,60]. This is indeed as we expect from the compact nature of TMA^+. Quantitative agreement with our simulated data is however not found, our τ_{rot} of 5 ps would correspond to τ_c of 0.8 ps. In this case, we consider the experimental value as less reliable due to the difficulty of decoupling the TMA^+ global rotation and methyl rotation as the characteristic times are very close, unlike for TBA^+. For completeness, experimental methyl rotational time ($\tau_{rot} \sim$) is 1-5 ps depending on the system studied and technique employed[13,50,61]. A difference in terminal methyl group rotation has already been reported in a low temperature NMR study, leading to a correlation time in case of TBA^+ a factor of six larger than in case of TMA^+[62]. The measurements of global as well as terminal methyl group rotation for TAA ions is a priori also available from quasi-elastic neutron scattering. However, the main and serious difficulty is, similarly to NMR, the decoupling of the different types of motion in the measured neutron signal, without the possibility to resorting to different nuclei (only H nuclei give measurable signal for these types of neutron scattering experiments). We have addressed this difficulty in detail in ref[43]. In conclusion, we were not able to extract global rotational times from our neutron scattering data.

Lastly, our MD simulations were able to reproduce well the experimental translational diffusion of TMA^+ and TBA^+, as well as water, across the concentration range studied. As our data show otherwise, the observed slowing down is not related to any cation aggregate formation, simple steric (obstruction) effects must be at the origin, as has already been suggested[11,24]. As it is a common observation that the results from classical simulations are influenced by the choice of the force field, overall we have paid a close attention to assessing the quality of the employed force field. We have presented three data sets supporting its realistic nature: a) the experimental density of TAABr solutions over a wide range is reproduced, b) dynamical properties (translational and rotational diffusion) is within good agreement of experimental data, c) when available neutron and X-ray scattering data is surprisingly well reproduced (case of 1m TBABr solution). In our attitude, the direct agreement with several experimental data sets is a very convincing argument in favour of the chosen force field.

5 Conclusion

In conclusion, we have discussed the structural and dynamic properties of aqueous TMABr and TBABr solutions across a wide range of concentrations (0.5 to 3-4 molal). With the help of detailed all-atom molecular dynamics simulations we are able to address aspects of ion hydration, ion dynamics and ion-ion interactions, while highlighting the steric details of the cations involved, contrasting the compact nature of TMA^+ and the penetrable nature of TBA^+. We have presented our results in light of the controversial cation-cation aggregation. Based on both structural and dynamic information regarding the TAA cations, we see no evidence for cation-cation aggregation in the systems studied. A well-established hydration is seen for both TMA^+ and TBA^+ throughout the concentration range studied. Both water molecules and counterions occupy the space between the hydrocarbon arms of TBA^+, which are found to remain in an extended configuration, whatever the concentration studied. At a given concentration, we observe a weaker cation-cation correlation in case of the TBA^+ ions in comparison to TMA^+ ions. We interpret this as a "softer" interaction between the bigger penetrable ions. Up to the respective one hydration sphere limits, we observe a concentration independent global rotation for both TMA^+ and TBA^+, which again points against any cation-cation aggregation. Beyond this limit, TBA^+ rotation is severely hindered and the origin is in the increasing inter-penetration of adjacent ions. Overall, without resorting to hydrophobicity, steric effects of TMA^+ and TBA^+ cations seem sufficient to explain to a great extent the differences in the microscopic (local) behaviour of their solutions. Other types of local features in concentrated TAA halide solutions, such as slowing down of water reorientation as probed by infrared spectroscopy[22], should also be viewed along these lines. A more appropriate description of larger TAA ions could simply be "bulky non-spherical penetrable ions". If, on top of steric features, hydrophobicity of the short hydrocarbon arms demonstrates itself, could it be masked by the effect of charge, at least for certain local properties? Looking for stark signature of hydrophobicity in local properties in order to explain the macroscopic thermodynamic data is perhaps a lost cause. Interestingly, we have observed recently that for ionene polyelectrolytes (long hydrocarbon chains with regular TAA charged centers), the effects of hydrophobicity are also suppressed to a surprising degree in their aqueous solutions, at least when certain structural features are considered[63].

6 Acknowledgements

The authors are very grateful to Bernard Ancian for NMR measurements and Emmanuelle Dubois, Werner Kunz, Jan Heyda and Pavel Jungwirth for fruitful discussions on tetraalkylammonium ions.

References

1 W.-Y. Wen, *Water and Aqueous Solutions. Structure, Thermodynamics, and Transport Processes*, John Wiley & Sons, New-York, 1972, ch. 15,

pp. 613–661.
2 W. Wen, *J. Solution Chem.*, 1973, **2**, 253–276.
3 Y. Marcus, *J. Solution Chem.*, 2008, **37**, 1071–1098.
4 H. Nakayama, H. Kuwata, N. Yamamoto, Y. Akagi and H. Matsui, *B. Chem. Soc. JPN.*, 1989, **62**, 985–982.
5 J. Turner, A. K. Soper and J. L. Finney, *Mol. Phys.*, 1990, **70**, 679–700.
6 J. Turner, A. K. Soper and J. L. Finney, *Mol. Phys.*, 1992, **77**, 411–429.
7 J. Turner and A. K. Soper, *J. Chem. Phys.*, 1994, **101**, 6116–6125.
8 J. T. Slusher and P. T. Cummings, *J. Phys. Chem. B*, 1997, **101**, 3818–3826.
9 L. García-Tarrés and E. Guàrdia, *J. Phys. Chem. B*, 1998, **102**, 7448–7456.
10 H. Hertz, B. Lindman and V. Siepe, *Ber. Bunsenges. Phys. Chem.*, 1969, **73**, 542–549.
11 P.-O. Eriksson, G. Lindblom, E. Elliott Burnell and G. J. T. Tiddy, *J. Chem. Soc., Faraday Trans. 1*, 1988, **84**, 3129–3139.
12 S. Bradl and E. W. Lang, *J. Phys. Chem.*, 1993, **97**, 10463–10471.
13 S. Bradl, E. W. Lang, J. Z. Turner and S. A. K, *J. Phys. Chem.*, 1994, **98**, 8161–8168.
14 B. Liegl, S. Bradl, T. Schätz and E. W. Lang, *J. Phys. Chem.*, 1996, **100**, 897–904.
15 A. G. Novikov, M. N. Rodnikova and O. V. Sobolev, *J. Mol. Liq.*, 2001, **91**, 91–97.
16 J. Z. Turner, A. K. Soper and J. L. Finney, *J. Chem. Phys.*, 1995, **102**, 5438–5443.
17 A. K. Soper, J. Turner and J. L. Finney, *Mol. Phys.*, 1992, **77**, 431–437.
18 P. Calmettes, W. Kunz and P. Turq, *Physica B*, 1992, **180**, 868–870.
19 N. G. Polydorou, J. D. Wicks and J. Z. Turner, *J. Chem. Phys.*, 1997, **107**, 197–204.
20 W. Kunz, P. Calmettes, T. Cartailler and P. Turq, *J. Chem. Phys.*, 1993, **99**, 2074–2078.
21 N. Huang, D. Schlesinger, D. Nordlund, C. Huang, T. Tyliszczak, T. M. Weiss, Y. Acremann, L. G. M. Pettersson and A. Nilsson, *J. Chem. Phys.*, 2012, **136**, 074507.
22 S. T. van de Post, S. Scheidelaar and H. J. Bakker, *J. Phys. Chem. B*, 2013, **117**, 15101–15110.
23 D. Chandler, *Nature*, 2005, **437**, 640–647.
24 G. Stirnemann, F. Sterpone and D. Laage, *J. Phys. Chem. B*, 2011, **115**, 3254–3262.
25 J. L. Green, M. G. Sceats and A. R. Lacey, *J. Chem. Phys.*, 1987, **87**, 3603–3610.
26 W. Smith, T. R. Forester and I. T. Todorov, *THE DL POLY 2 USER MANUAL*, Version 2.18, STFC Daresbury Laboratory, UK, 2007.
27 M. P. Allen and D. J. Tildesley, *Computer Simulations of Liquids*, Oxford University Press, 1989.
28 J. Heyda, M. Lund, M. Oncák, P. Slavícek and P. Jungwirth, *J. Phys. Chem. B*, 2010, **114**, 10843–10852.
29 T. Hrobárik, L. Vrbka and P. Jungwirth, *Biophys. Chem.*, 2006, **124**, 238–242.
30 W. D. Cornell, P. Cieplak, C. I. Bayly, I. R. Gould, K. M. Merz, D. M. Ferguson, D. C. Spellmeyer, T. Fox, J. W. Caldwell and P. A. Kollman, *J. Am. Chem. Soc.*, 1995, **117**, 5179–5197.
31 L. Vrbka and P. Jungwirth, *Aust. J. Chem.*, 2004, **57**, 1211–1217.
32 D. Case, T. A. Darden, T. E. Cheatham, III, C. L. Simmerling, J. Wang, R. E. Duke, R. Luo, M. Crowley, R. C. Walker, W. Zhang, K. M. Merz, B. Wang, S. Hayik, A. Roitberg, G. Seabra, I. Kolossvry, K. F. Wong, F. Paesani, J. Vanicek, X. Wu, S. R. Brozell, T. Steinbrecher, H. Gohlke, L. Yang, C. Tan, J. Mongan, V. Hornak, G. Cui, D. H. Mathews, M. G. Seetin, C. Sagui, V. Babin and P. A. Kollman, *AMBER 10*, University of California, San Francisco, 2008.
33 S. Koneshan, J. C. Rasaiah, R. M. Lynden-Bell and S. H. Lee, *J. Phys. Chem. B*, 1998, **102**, 4193–4204.
34 D. Horinek, S. Mamatkulov and R. Netz, *J. Chem. Phys.*, 2009, **130**, 124507.
35 S. H. Lee and J. C. Rasaiah, *Biophys. Chem.*, 1996, **100**, 1420–1425.
36 I. S. Joung and T. E. Cheatham, *J. Phys. Chem.*, 2008, **112**, 9020–9041.
37 G. Markovich, L. Perera, M. L. Berkowitz and O. Cheshnovsky, *J. Chem. Phys.*, 1996, **7**, 2675–2685.
38 H. J. C. Berendsen, J. R. Grigera and T. P. Straatsma, *J. Phys. Chem*, 1987, **91**, 6269–6271.
39 D. Frenkel and B. Smit, *Understanding Molecular Simulation, From Algorithms to Applications*, Academic Press, 2nd edn, 2002, ch. 12, pp. 291–320.
40 J.-P. Ryckaert, G. Ciccotti and H. J. Berendsen, *J. Comput. Phys.*, 1977, **23**, 327–341.
41 G. R. Kneller, V. Keiner, M. Kneller and M. Schiller, *Comput. Phys. Commun.*, 1995, **91**, 191–214.
42 T. Róg, K. Murzyn, K. Hinsen and G. R. Kneller, *J. Comput. Chem.*, 2003, **24**, 657–667.
43 D. Bhowmik, N. Malikova, J. Teixeira, G. Mériguet, O. Bernard, P. Turq and W. Häußler, *Eur. Phys. J. Special Topics*, 2012, **213**, 303–312.
44 I.-C. Yeh and G. Hummer, *J. Phys. Chem. B*, 2004, **108**, 15873–15879.
45 S. Tazi, A. Boţan, M. Salanne, V. Marry, P. Turq and B. Rotenberg, *J. Phys.: Condens. Matter*, 2012, **24**, 284117.
46 B. J. Berne and R. Pecora, *Dynamic light scattering: with applications to chemistry, biology, and physics*, Wiley, New York, 1975.
47 M. Bée, *Quasielastic Neutron Scattering: Principles and Applications in Solid State Chemistry, Biology and Material Science*, Adam Hilger, Bristol and Philadelphia, 1988, ch. 6, pp. 176–249.
48 D. E. Woessner, *J. Chem. Phys.*, 1962, **36**, 1–4.
49 J. Kowalewski and L. Mäler, *Nuclear Spin Relaxation in LiquidsTheory, Experiments, and Applications*, Taylor & Francis, 2006, ch. 6, pp. 127–157.
50 J. T. Cabral, A. Luzar, J. Teixeira and M. C. Bellissent-Funel, *J. Chem. Phys.*, 2000, **113**, 8736–8745.
51 H. Krienke, V. Vlachy, G. Ahn-Ercan and I. Bakó, *J. Phys. Chem. B*, 2009, **113**, 4360–4371.
52 E. Hawlicka and T. Dlugoborski, *Chem. Phys. Lett.*, 1997, **268**, 325–330.
53 R. Buchner, C. Holzl, J. Stauber and J. Barthel, *Phys. Chem. Chem. Phys.*, 2002, **4**, 2169–2179.
54 J. R. Lyerla and G. C. Levy, *Topics in Carbon-13 NMR Spectroscopy*, John Wiley & Sons, 1974, vol. 1, ch. 3, pp. 79–148.
55 H. Hertz and M. Zeidler, *Ber. Bunsenges. Phys. Chem.*, 1964, **68**, 821–837.
56 T. W. McGaughy, S. Y. C. Wu and B. M. Fung, *J. Chem. Phys.*, 1978, **69**, 473–478.
57 Y. Masuda, J. Tobita and A. Muramoto, *Bull. Chem. Soc. Jpn.*, 1998, **71**, 1555–1563.
58 Y. Masuda and A. Muramoto, *J. Solution Chem.*, 2004, **33**, 811–825.
59 M. Holz and K. J. Patil, *Ber. Bunsenges. Phys. Chem.*, 1991, **95**, 107–113.
60 F. Sacher, M. Holz and H. Hertz, *J. Magn. Reson. A*, 1993, **103**, 61–71.
61 P. J. Bratt, D. G. Gilles, L. H. Sucliffe and A. J. Williams, *J. Phys. Chem.*, 1990, **94**, 2727.
62 E. W. Lang, S. Bradl, W. Fink, H. Radkowitsch and D. Girlich, *J. Phys.: Condens. Matter*, 1990, **2**, SA195–SA200.
63 N. Malikova, S. Cebasek, V. Glenisson, D. Bhowmik, G. Carrot, V. Vlachy, *Phys. Chem. Chem. Phys.*, 2012, **14**, 12898–12904.

7 Figures and Tables

System	Composition cat - ani - H_2O	Box Size [Å]	MD length [ns]	Molar Ratio ions:H_2O	molality (m) [mol kg^{-1}]	molarity (M) [mol dm^{-3}]
TMABr	8 - 8 - 176	18.92	3.4	1:22	2.52 (*)	2.01
	8 - 8 - 352	22.93	3.4	1:44	1.26	1.12
	8 - 8 - 448	24.65	3.4	1:56	0.99	0.90
	8 - 8 - 528	25.87	3.4	1:66	0.84	0.77
	8 - 8 - 704	28.27	3.4	1:88	0.63	0.59
TBABr	8 - 8 - 112	19.42	3.4	1:14	3.96	1.83
	24 - 24 - 336	28.17 [L]	16.4	1:14	3.96	1.83
	8 - 8 - 224	21.97	3.4	1:28	1.98	1.25
	8 - 8 - 448	25.90	3.4	1:56	0.99 (*)	0.77
	16 - 16 - 896	32.54	16.4	1:56	0.99	0.77
	24 - 24 - 1344	37.35 [L]	3.4	1:56	0.99 (*)	0.77
	8 - 8 - 896	31.39	3.4	1:112	0.50	0.43
	1 - 1 - 896	30.14	8.2	1:896	isolated (0.06)	isolated (0.06)
NaBr	8 - 8 - 448	24.07	3.4	1:56	0.99	0.97

Table 1 Overview of simulated systems. "Composition" indicates the total contents of the simulation box, in terms of the numbers of cations, anions and water molecules. "Box Size" stands for the length of the side of the cubic box, it is determined by MD simulations in an NPT ensemble (T=298K, p=1bar). [L] indicates large box simulations for a chosen set of concentrations. "MD length" is the length of the collected simulated trajectory in the NVE ensemble used for further analysis. Asterisk (*) indicates the concentration formally considered to be just sufficient for the formation of a single hydration shell per cation.

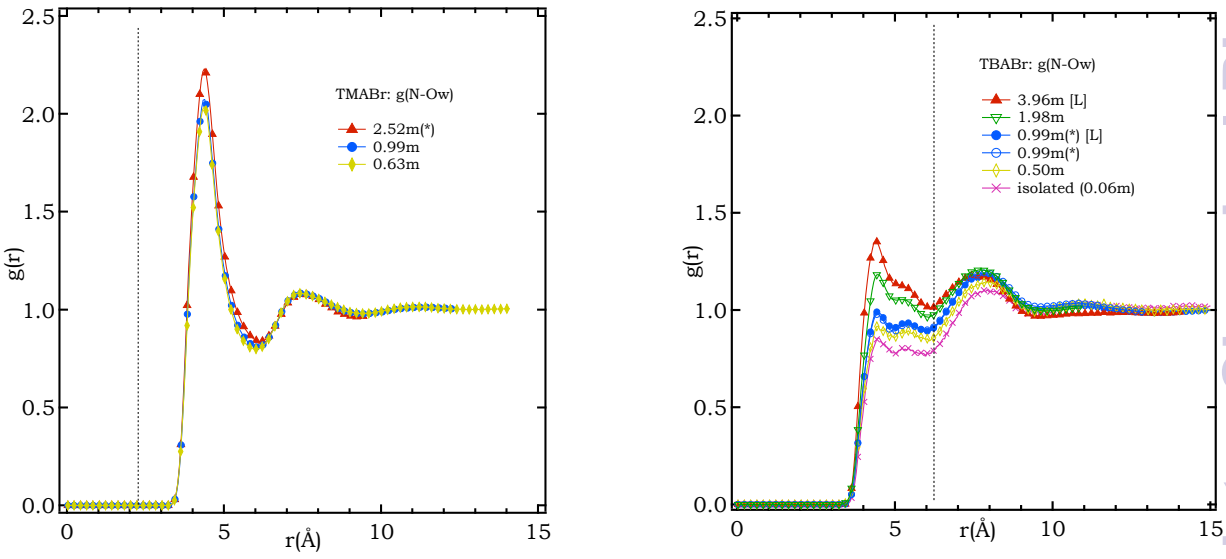

Fig. 1 Radial distribution function between the nitrogen atoms of cations and the oxygen atoms of water molecules, g_{NOw}, for TMABr solutions (left) and TBABr solutions (right) for a series of concentrations as indicated. Vertical dotted lines indicate the position of the outermost hydrogen atoms of the cation. Symbol [L] indicates the use of large simulation boxes for certain concentrations, refer back to Table 1. Asterisk (*) indicates the concentration formally considered to be just sufficient for the formation of a single hydration shell per cation.

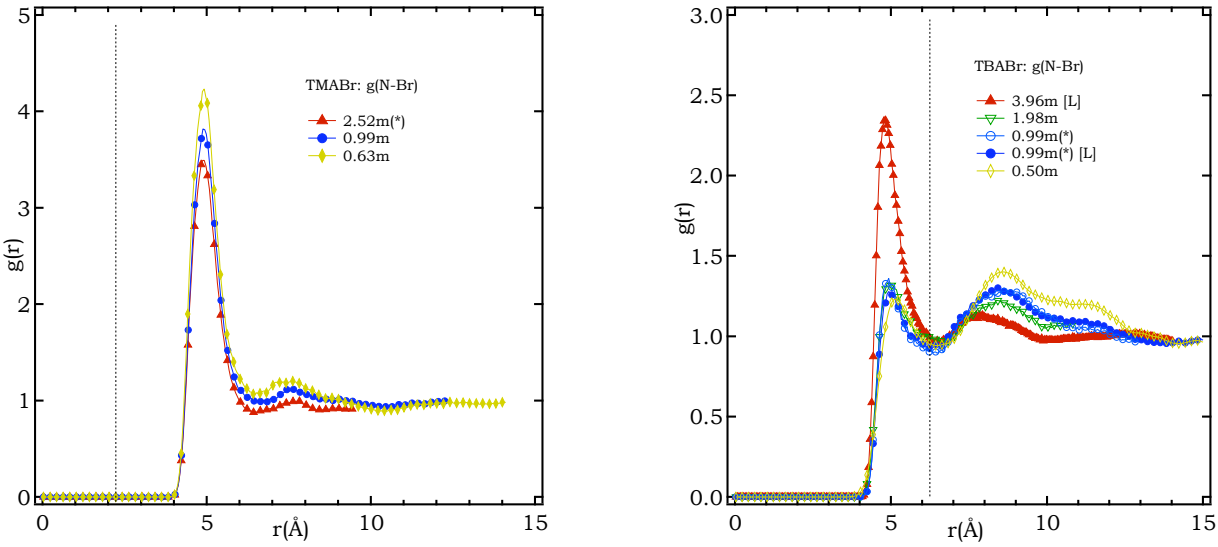

Fig. 2 Radial distribution function between the nitrogen atom of the cation and the bromide anion, g_{NBr}, for TMABr solutions (left) and TBABr solutions (right) for a series of concentrations as indicated. Vertical dotted lines indicate the position of the outermost hydrogen atoms of the cation. Symbol [L] for the TBABr systems indicates the use of large simulation boxes.

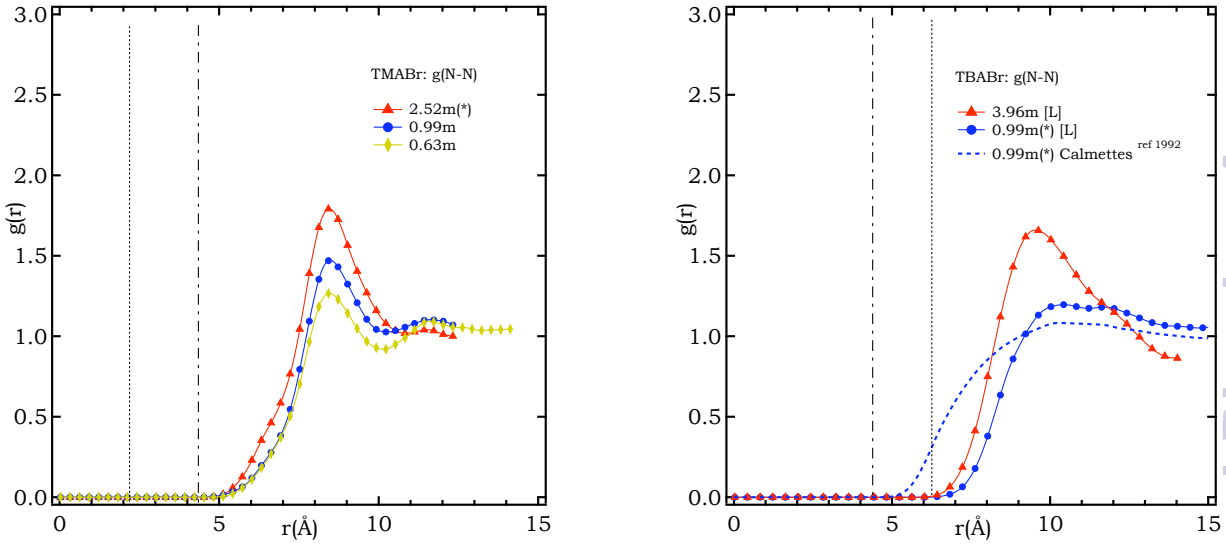

Fig. 3 Radial distribution function between the nitrogen atoms of cations, g_{NN}, for TMABr solutions (left) and TBABr solutions (right) for a series of concentrations as indicated. Symbol [L] indicates the use of large simulation boxes. Dotted and dashed-dotted vertical lines indicate, respectively, position of the outermost hydrogen atoms of the cation and position of the first peak in g_{NOw}. Dashed blue series on the right Figure corresponds to data from a TBA-TBA potential derived from hypernetted chain (HNC) calculations in ref[18].